SAND2018-9624C

The Effect of Bulk Gas Diffusivity on Apparent Pulverized Coal Char Combustion Kinetics

Christopher R. Shaddix, Ethan S. Hecht, Cristina Gonzalo-Tirado[†], and Brian S. Haynes[‡]

Combustion Research Facility
Sandia National Laboratories
Livermore, California 94550

Abstract

Apparent char kinetic rates are commonly used to predict pulverized coal char burning rates. These kinetic rates quantify the char burning rate based on the temperature of the particle and the oxygen concentration at the external particle surface, inherently neglecting the impact of variations in the internal diffusion rate and penetration of oxygen. To investigate the impact of bulk gas diffusivity on these phenomena during Zone II burning conditions, experimental measurements were performed of char particle combustion temperature and burnout for a subbituminous coal burning in an optical entrained flow reactor with helium and nitrogen diluents. The combination of much higher thermal conductivity and mass diffusivity in the helium environments resulted in cooler char combustion temperatures than in equivalent N_2 environments. Measured char burnout was similar in the two environments for a given bulk oxygen concentration but was approximately 60% higher in helium environments for a given char combustion temperature. To augment the experimental measurements, detailed particle simulations of the experimental conditions were conducted with the SKIPPY code. These simulations also showed a 60% higher burning rate in the helium environments for a given char particle combustion temperature. To differentiate the effect of enhanced diffusion through the external boundary layer from the effect of enhanced diffusion through the particle, additional SKIPPY simulations were conducted under selected

conditions in N_2 and He environments for which the temperature and concentrations of reactants (oxygen and steam) were identical on the external char surface. Under these conditions, which yield matching apparent char burning rates, the computed char burning rate for He was 50% larger, demonstrating the potential for significant errors with the apparent kinetics approach. However, for specific application to oxy-fuel combustion in CO_2 environments, these results suggest the error to be as low as 3% when applying apparent char burning rates from nitrogen environments.

Keywords: coal; char; combustion; kinetics; diffusion

† Present address: Research Centre for Energy Resources and Consumption (CIRCE), Universidad de Zaragoza, Mariano Esquillor Gómez, 15, 50018 Zaragoza, Spain.

‡ School of Chemical and Biomolecular Engineering, University of Sydney, NSW 2006, Australia

1. Introduction

The competition between oxygen penetration and consumption during the combustion of porous pulverized char particles has long been recognized as an important aspect of quantifying the char burning rate [1-3] and the basic approach to this problem dates back to Thiele's description of reactions in porous catalysts [4]. Unfortunately, it is extremely difficult to experimentally quantify the extent of oxygen penetration during char burnout under practical high temperature combustion conditions. Consequently, 'apparent' char kinetic expressions, which relate the char consumption rate to the external diameter of the particle, the temperature of the particle, and the oxygen partial pressure on the external surface of the particle, as shown in Eq. 1-2, are frequently employed, particularly in large CFD (computational fluid dynamic) calculations of pulverized coal combustion [5-9].

$$q = k_s p_{O_{2,s}}^{n} \qquad \text{Eq. 1}$$

$$k_s = Aexp\left(-E/RT_p\right) \quad \text{Eq. 2}$$

with q giving the mass or molar consumption rate of carbon per unit external surface area of the particle. However, since the apparent kinetics approach does not explicitly model the reaction-diffusion flux within the particle, it necessarily presumes that the *relative* penetration of oxygen (and thereby its accessibility to internal reactive surface area of the particle) is invariant during burnout and even during combustion at different temperatures, for different external surface oxygen concentrations, or with a different diluent gas, for a given type of coal char.

To gain better insight into the influence of oxygen penetration and internal diffusivity on apparent char kinetic oxidation rates under practical combustion conditions, we have performed a series of char kinetic experiments for pulverized coal char particles in nitrogen and helium bath gases. As shown in Fig. 1, oxygen has a much greater diffusivity in helium than in nitrogen, by a factor of approximately 3.5 over the temperature range of 300-2000 K. Furthermore, as shown in Fig. 2, the thermal conductivity of helium is also much higher than that of nitrogen (by a factor of approximately 5). Experimentally, as will be shown later, we find that the combination of high diffusivity and high thermal conductivity of helium results in char particle combustion temperatures in helium that are lower, but with similar trends, to those in nitrogen. For this reason, comparing the char reaction rates in nitrogen and helium can give good insight into differences in apparent and actual reactivity, particularly in combination with detailed intrinsic char combustion modeling.

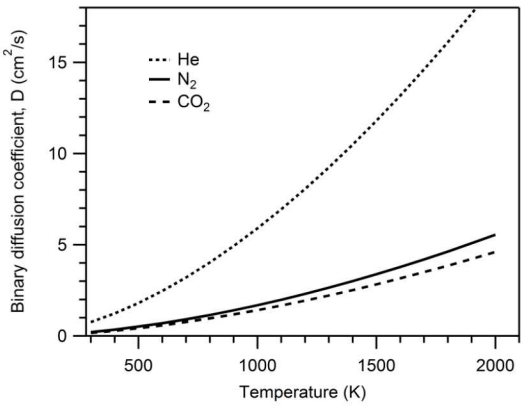

Figure 1. Binary diffusion coefficient of oxygen in He, N_2, and CO_2 as a function of temperature, computed using correlations from Marrero and Mason [10].

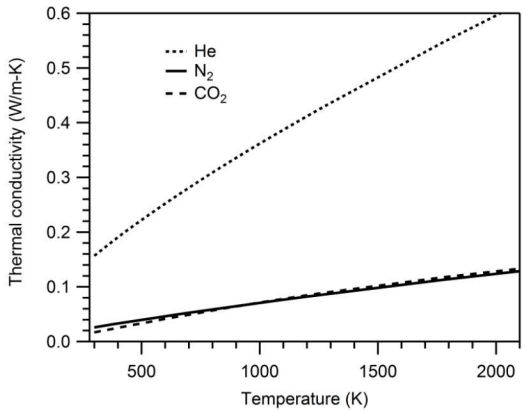

Figure 2. Thermal conductivity of He, N_2, and CO_2 as a function of temperature, according to the correlations published by Kestin et al. [11] for He and by Uribe et al. [12] for the polyatomic gases.

Figures 1-2 also show the diffusivity and thermal conductivity of CO_2, as these properties are relevant to oxy-fuel combustion, wherein oxygen is mixed with predominately CO_2. As is evident in Fig. 1, the diffusivity of oxygen in CO_2 is 17% lower than in N_2, whereas Fig. 2 shows the thermal conductivity of CO_2 is very similar to that of N_2. Because of the lower diffusivity of oxygen in CO_2, it is unclear what correction (if any) should be applied to apparent char oxidation

kinetic rates that have been measured for coal chars in conventional (O_2/N_2) environments when considering oxy-fuel combustion [13]. This consideration gives specific motivation for the study described here.

2. Experimental Methods

2.1 Entrained flow reactor

Sandia's combustion-driven optical entrained flow reactor was utilized for this study. This reactor has been well characterized and the details of its operation and its utility for char kinetic determinations have been previously reported [6]. A particle-sizing pyrometer was utilized, as described previously, to perform measurements of the char particle size, temperature, and velocity for entrained char particles burning in isolation from one another. Char particle temperature measurements provide critical information on the actual char combustion rate temperature and, in the absence of competing gasification reactions, can be used to directly derive apparent char combustion (oxidation) rates [6]. To assure good sampling statistics, between 100 and 150 good quality single-particle optical signal traces were collected for each of several selected sampling heights for a given reactor condition. The corresponding particle residence time in the laminar flow furnace was deduced from the measured mean char particle velocities (slight differences were evident for different flow conditions).

A N_2-quench, water-cooled isokinetic sampling probe was used to collect char samples at selected reactor heights for subsequent determination of char burnout. The refractory elements Si, Al, and Ti were measured commercially by ICP-OES (inductively coupled plasma optical emission spectrometry) and their concentrations were compared to those in the base char material to

calculate the burnout of the organic matter in the char, according to Eq. 3 (written for the case of Ti):

$$\left({}^{m}/_{m_0}\right)_{daf} = \left({}^{Y_{Ti}}/_{Y_{Ti,0}}\right) * {}^{\left[1 - Y_{ash,0} * \left(Y_{Ti}/Y_{Ti,0}\right)\right]}/_{\left(1 - Y_{ash,0}\right)} \qquad \text{Eq. 3}$$

Due to data scatter in the determination of burnout according to each refractory metal, the results from the three metals were averaged for the results presented here.

2.2 Furnace conditions

The choice of furnace operating conditions involved a complex balance of assuring consistent char particle ignition and combustion, while attempting to keep the char combustion temperatures low enough to minimize or eliminate contributions from boundary layer conversion of CO [14] and gasification reactions involving H_2O and CO_2 [15]. For this reason, a nominal furnace gas temperature of 1300 K was chosen, produced by operating the Hencken burner at an adiabatic flame temperature of approximately 1400 K. Three different oxygen concentrations were utilized: 12, 18, and 24 vol-% O_2, with a total furnace flow of 40 slpm. The dry (unheated) diluent gas that was used to deliver the char particles to the furnace was limited to 0.12 slpm for N_2 and to 0.20 slpm for He. It was observed that the helium diluent flows suffered substantially larger heat losses in the (upflow) reactor as a function of vertical position, presumably from increased thermal conduction to the unheated reactor walls. Consequently, the burner flame temperatures were fine-tuned such that the measured gas temperature at the furnace height where the peak char combustion temperature was observed was equal to approximately 1300 K for both helium and nitrogen diluents, as shown in Fig. 3. Note that balancing the gas temperature with the two diluents is not necessary for quantitative analysis of char kinetic rates, as the actual gas temperatures are included in the analysis. For the helium diluent, peak char combustion temperatures occurred at a height of

3 cm, compared to a height of 6 cm for nitrogen diluent. The gas temperature profiles were measured with a very fine wire (25 μm dia.) type-R thermocouple, corrected for radiant loss [16], which is very minor (~ 15 K) for such a fine thermocouple at this low temperature. The flow conditions are described in Table 1. Direct measurement of the helium flow through the metering critical flow orifice using laminar flow elements was performed after the optical measurements were completed and resulted in a minor adjustment to the indirectly calibrated flow rates. Consequently, slightly higher oxygen concentrations were used for the helium diluent experiments than for the nitrogen diluent experiments.

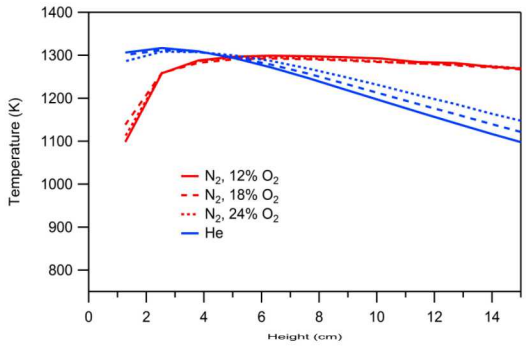

Figure 3. Centerline gas temperature profiles in the optical entrained flow reactor for the investigated flow conditions.

Table 1. Calculated composition of furnace gases (mol %)

	N_2_12	N_2_18	N_2_24	He_12	He_18	He_24
CO_2	2.5	2.3	2.8	1.2	1.2	1.0
H_2O	10.0	10.5	9.5	9.3	9.2	9.7
N_2	75.5	69.2	63.7			
He				77.1	71.2	64.7
O_2	12.0	18.0	24.0	12.4	18.4	24.6

2.3 Pulverized char particles

To assure a common char material for the particles in the different reactor environments, high heating rate char particles were first generated by feeding pre-sieved pulverized low-sulfur subbituminous coal (Black Thunder) particles at a low feed rate into a turbulent entrained flow reactor operating at 1200 °C and 1 atm with a preheated nitrogen flow with 1.5% O_2 (to prevent tar formation and condensation). The particles were exposed to the high-temperature environment for 250 ms to assure complete devolatilization, before being quenched by means of cool N_2 flow at the inlet of a water-cooled collection probe. The collected char was size-classified to several different size fractions using a mechanical sieve shaker. The 63-75 μm size cut was utilized in this study, after re-sieving the particles to remove any residual fines. The use of pre-formed, narrowly-sieved chars provides a well-known measure of the char particle diameter, at least for early extents of oxidation before the particles shrink, and precludes a reliance on optically measured particle diameters, which typically have an uncertainty of 20% and are limited to char particle sizes greater than 80 μm. Table 2 shows the ultimate and proximate analysis of the raw coal and the derived char particles. Based on a total ash tracer approach, the prepared char corresponds to 46% burnout of the raw coal.

3. Porous Reacting Particle Modeling

To augment the interpretation of the experimental measurements, we employed the Surface Kinetics in Porous Particle (SKIPPY) code [17,15] developed at the University of Sydney. SKIPPY solves the mass, species, and energy conservation equations inside and outside a porous particle reacting under steady-state conditions in a quiescent environment. From this solution, SKIPPY gives the gas species concentrations and temperature within the pores of the char, at the outer surface of the char, and within the layer of gas surrounding the char. Both heterogeneous

(gas-solid) and gas-phase chemical reactions are considered, by employing data and subroutines from the CHEMKIN [18], SURFACE CHEMKIN [19], and Sandia transport [20] packages. A solution is found through the TWOPNT [21] solver and mesh points are automatically added in regions with high gradients.

Table 2: Composition of Coal and Prepared Char

wt-%, DAF	coal	char
C	69.0	89.6
H	5.0	0.77
O	25.4	8.0
N	0.97	1.31
S	0.45	0.38
wt-%		
moisture	9.3	3.7
ash	4.8	9.5
volatiles	42.3	12.7
fixed C	43.6	74.1

For the calculations employed here, GRI-MECH 3.0 [22], without nitrogen reactions, was used to describe the gas-phase reaction kinetics. Several different surface mechanisms were investigated for the range of experimental conditions of this study to achieve numerical stability and reasonable agreement with the measured char combustion temperatures in the N_2 diluent. A combined oxidation/gasification mechanism applied previously by Hecht et al. [15] under high-temperature reaction conditions was tried first. However, it was not possible to reach a converged solution with that mechanism for gas temperatures below 1600 K, presumably because of the strong gradient between the hot particles and the relatively cool surroundings for the conditions investigated here. Subsequently, the gasification rates used by Hecht et al. [15] were decreased by a factor of two, which is still within the level of uncertainty of such rates at high temperatures. This choice yielded converged solutions over the range of experimental conditions and was used

for the analysis presented here, though the predictions overestimate the char temperature rise with increasing oxygen content. This behavior has been observed previously when underestimating the contribution of gasification reactions during char combustion [7,14,15]. To mitigate this, the assumed tortuosity in the calculations for the 12% O_2 condition was reduced to 2, compared to the value of 4 presumed for the other flow conditions. The mechanism used is shown in Table 3, wherein, as in previous uses of SKIPPY [14,15,17], the oxidation and gasification reactions are treated as adsorption-limited, with arbitrarily fast desorption reaction rates that guarantee insignificant accumulation of oxygen complexes on the char surface. Further optimization of the SKIPPY predictions relative to the measured char particle temperatures would undoubtedly be possible by increasing the magnitude of the gasification rates, but this is not expected to materially influence the derived trends from the simulations and thus was not pursued.

Table 3: Heterogeneous Oxidation and Gasification Mechanism

Reaction	A (units of mol,cm,s)	E (kJ/mol)
$C_b + C_s + O_2 \rightarrow CO + C(O)_s$	3.30×10^{15}	167.4
$C(O)_s + C_b \rightarrow CO + C_s$	1.00×10^{8}	0
$C_s + O_2 \rightarrow C(O_2)_s$	9.50×10^{13}	142.3
$C(O_2)_s + C_b \rightarrow CO_2 + C_s$	1.00×10^{8}	0
$C_s + CO_2 \rightarrow CO + C(O)_s$	1.80×10^{15}	251.0
$C_s + H_2O \rightarrow H_2 + C(O)_s$	2.17×10^{14}	222.0

4 Results and Discussion

4.1 Char particle combustion temperatures

Figure 4 shows the char particle temperatures measured in the N_2 and He diluent environments, as a function of char particle residence time, together with the calculated char particle temperatures from the SKIPPY simulations. For reference purposes, a height of 5 cm in the reactor corresponds to a residence time of 38 ms. The experimental data are shown as box-and-whisper plots to indicate

the statistical distribution of measured char temperatures at each axial position for a given flow condition. The size of the 25-75 percentile box edges (i.e. the H-spread) of the measurements indicates the combined effects of the 2-color pyrometry precision and the variation in the size and composition (reactivity) of the char feed particles. For the measurements performed during intermediate stages of burnout the H-spread is quite small (on the order of 20-30 K). The H-spread is enlarged at the edges of the measurement heights, as expected, where incompletely ignited particles (at low heights) or partly extinguished particles (at high heights) are likely present within the measured particle population.

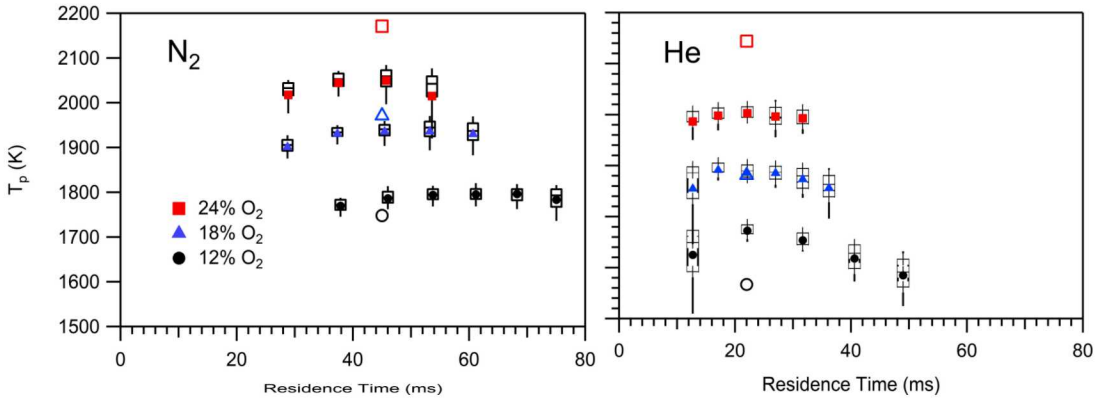

Fig. 4 Measured and modeled char particle temperatures as a function of residence time in the entrained flow reactor for N_2 and He diluents. The mean particle temperatures are shown as symbols, whereas the box and whiskers surrounding the data points indicate the 25-75 percentile limits (box edges) and the 10-90 percentile limits (whiskers) of the measured distribution at each sampling location. The open symbols indicate the char particle temperatures calculated by SKIPPY for the corresponding gas conditions. The SKIPPY prediction for 18% O_2 in He lies almost perfectly on top of the experimental data and therefore is difficult to discern.

Figure 4 shows a strong dependence of char combustion temperature on the oxygen concentration of the furnace gas, for both diluent gases, as expected [6-7,14-15]. It is also apparent that the char particles ignite much more quickly in the helium environment than in the N_2

environment. A faster ignition in helium is also expected, based on both the improved O_2 diffusivity through helium as well as helium's high thermal conductivity. These two factors act in tandem to rapidly heat the gas surrounding the particles (and the particles themselves) while also rapidly transporting oxygen to the particle surface to initiate exothermic oxidation reactions [23]. For a given bulk O_2 concentration, the char combustion temperature in helium is consistently lower than in N_2, by 100–150 K, reflecting the high thermal conductivity in helium, which effectively cools the particles through conductive heat loss and more than offsets the additional chemical heat release in He due to the higher diffusivity of oxygen to the particle surface.

4.2 Char burnout

Figure 5 shows the measured burnout, as determined from char collection and analysis via the refractory ash tracer technique. Even after averaging the three measured refractory metals, there is significant noise evident in the profiles. Due to the difficulty in collecting sufficient sample mass for analysis when feeding char particles at such a low feed rate to assure isolated particle combustion, only single samples were collected at each height. Table 4 shows the values of the line fits that were determined for the different experimental conditions, as well the burning rates calculated from the SKIPPY modeling. A direct comparison between the SKIPPY rates and the experimental rates is not possible, because of ambiguity over the experimental and modeled char densities, particularly as the experimental char burns out. However, the experimental and computational trends are similar, specifically for a given diluent gas.

It is apparent that the experimental burning rates are quite similar for the chars burning in the nitrogen and helium environments *for a given oxygen concentration*. However, the lower char combustion temperatures in the helium environments, coupled with the similar mass burning rates,

implies that the char temperature-normalized burning rate is significantly greater in the helium environments, as expected, because of the greater diffusivity of O_2 in He. Of course, that increased burning rate is the result of enhanced diffusive transport of oxygen to the particle surface, in addition to any enhancement resulting from enhanced diffusive transport within the char particle, so we must rely on modeling to decouple these effects and understand the impact of gas diffusivity on apparent burning rate.

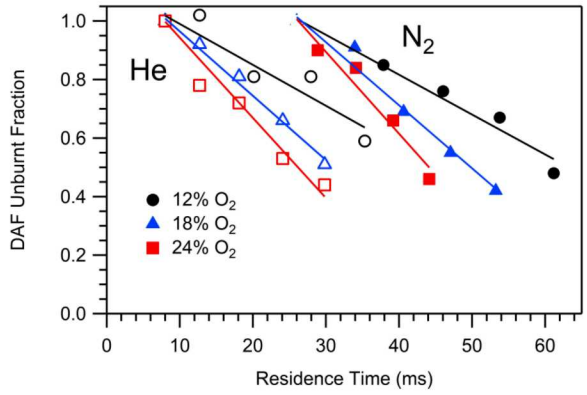

Fig. 5 Measured dry, ash-free burnout of the char particles as a function of residence time in the entrained flow reactor for N_2 and He diluents. Line fits to the data are shown.

Table 4: Char Burning Rates

Diluent Gas	Oxygen Concentration	Experimental Burning Rate (1/s)	Calculated Burning Rate (10^{-8} mol/s)
N_2	12.0 vol-%	13.6	4.7
	18.0 vol-%	21.5	8.0
	24.0 vol-%	27.9	12.3
He	12.4 vol-%	14.0	6.6
	18.4 vol-%	22.0	11.3
	24.6 vol-%	27.4	17.7

4.3 SKIPPY results

Figure 6 shows computed profiles of temperature and reacting gas species for the 18% O_2 cases. Greater penetration of O_2 into the char particle is evident in the He environment, as well as smoother gas profiles, because of the greater He diffusivity. At least a portion of the greater char penetration of O_2 in He environments can be ascribed to the higher concentration of O_2 on the particle surface. For the 18% O_2 cases shown in Fig. 6, $[O_{2,s}]$ is equal to 0.030 for the N_2 diluent gas and 0.057 for He diluent. CO_2 and H_2O penetrate to the center of the particle in both environments, because of their much lower reactivity than O_2. The SKIPPY calculations show a 1% contribution of the gasification reactions to conversion of the char for the case of 18% O_2 in He and a 9% contribution for the equivalent N_2 environment (the greater impact results from the higher char temperature). While the effect of the gasification reactions on the char conversion rate is low, particularly for O_2 levels below 24%, these reactions do have a significant impact on the char particle temperatures, as previously reported [7,14,15].

SKIPPY also calculates the O_2 effectiveness factor and the overall carbon consumption rate. When these entities are plotted against the bulk O_2 content of the gas, both the effectiveness factor and the carbon consumption rate are approximately a factor of two higher for the He diluent relative to N_2. However, as shown in Fig. 7, when plotted against the particle temperatures, the effectiveness factors collapse onto a common curve, whereas the carbon consumption rate remains much higher for the He diluent. Interestingly, when considering Fig. 4, it is evident that the experimentally measured char combustion temperatures in 18% O_2 in He are nominally at 1800 K, the same temperature as char particles burning in 12% O_2 in N_2. When comparing the measured char burning rates in Table 4, this implies the burning rate at a given char particle temperature is

greater in He by a factor of 22.0/13.6 = 1.6, which is equal to the ratio of 1.6 found for the slopes in line fits to the carbon consumption trends shown in Fig. 7.

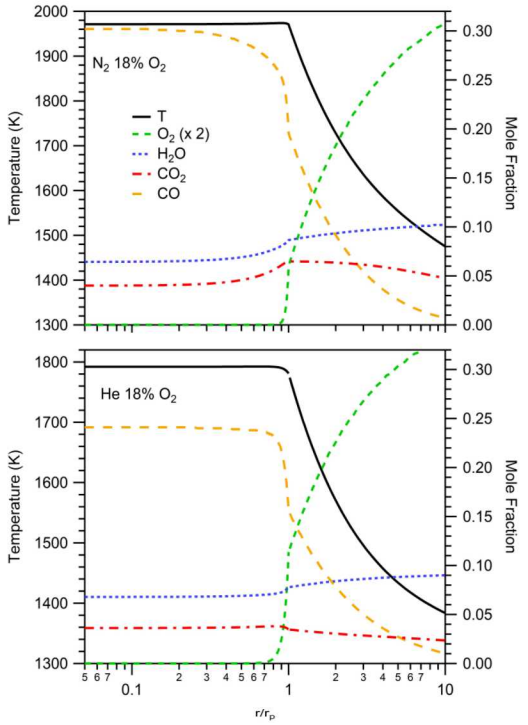

Fig. 6 Computed temperature and gas species profiles for 70 μm char particles reacting in the 18% O_2 mixtures described in Table 1 at a gas temperature of 1300 K.

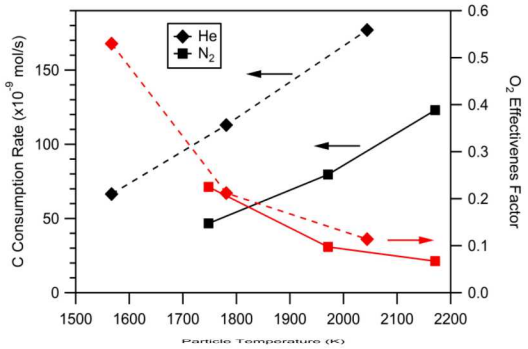

Fig. 7 Computed carbon consumption rates and O_2 effectiveness factors as a function of particle temperature for 70 μm char particles reacting in 1300 K gases, per the experimental conditions described in Table 1.

As discussed before, however, one needs to account for the oxygen concentration at the external particle surface, and not just the particle temperature, to deduce the effect of gas diffusivity on the apparent kinetic rate. To address this issue, we have modified the calculation for the He diluent to generate a burning char particle with the same temperature and surface oxygen concentration as calculated for the case of 18% O_2 in N_2. To simplify the comparison, we assume 10% H_2O in the bulk gas for both cases, and no bulk gas CO_2 content. To increase the char particle temperature in the He environment to match that in the N_2 environment, we increased the radiant flux to the particle by raising the 'wall' temperature of the radiant boundary in the SKIPPY calculation. To reduce the surface oxygen concentration in the He environment, which tended to be somewhat higher than in the N_2 environment, the O_2 content in the bulk gas was reduced. Through trial-and-error, we found that we could reproduce the desired char burning conditions in He for a bulk O_2 content of 13.3% and a radiant wall temperature of 2790 K. Fortuitously, the H_2O concentration at the external particle surface under these conditions matched that under the N_2 environment. Though the external boundary conditions vary between the N_2 and He calculations, at the char particle surface both calculations treat a char particle with a surface temperature of 1983 K, an oxygen concentration of 2.94%, and a water vapor concentration of 8.2%. Therefore, according to the apparent kinetics approach, the two computed particles should have the same reaction rate (ref. Eqs. 1-2).

The temperature and main gas concentration profiles internal to the particle for these two calculations are shown in Fig. 8, in an expanded scale. The primary difference in the two cases is the lower CO and CO_2 concentrations in the He bath gas, a consequence of the high diffusivity of gases in He, which prevents these product gases from building up to the concentrations seen in the N_2 case. Slightly greater penetration of O_2 is evident in the He bath gas, but it is a very small

difference. Still, the calculated char oxidation rate is 50% higher in helium, a consequence of the higher flux of O_2 into the particle. As a sanity check, the calculated oxidation rate of the external char *surface* is the same for these two char particles, as it should be, given the identical char surface temperature and oxygen concentration.

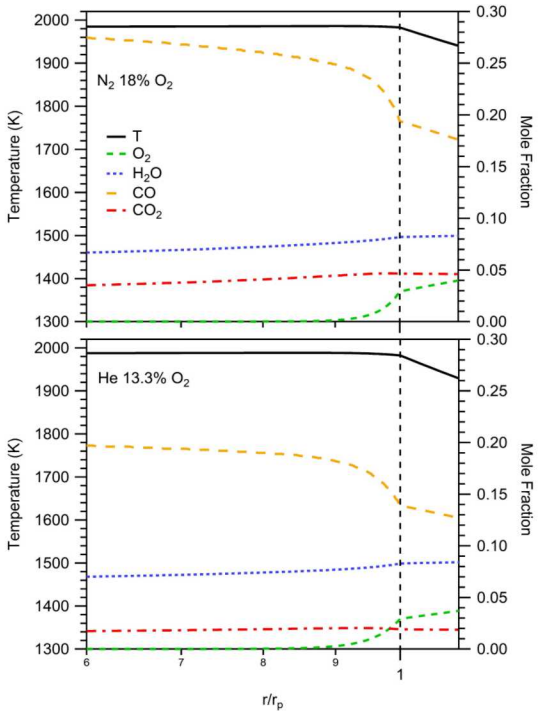

Fig. 8 Computed gas temperature and gas species profiles within and just outside the surface of 70 μm char particles reacting in 1300 K gases in N_2 and He environments with 10% H_2O. For the He case, the radiant boundary condition is at 2790 K and the bulk O_2 content is 13.3%, whereas the radiant boundary is 600 K and the bulk O_2 content is 18% for the N_2 case.

The similar extent of char penetration by O_2 in the He and N_2 environments under these matched external particle conditions is an unexpected result, but understandable given the enhanced flux of oxidation/gasification products out of the char particle in the more diffusive He environment, which works to offset the increased O_2 penetration that would otherwise occur. This

result shows that the correct way to think about the effect of gas diffusivity is in terms of the *flux* of reactants (and products), rather than in terms of char penetration.

As shown by these simulations with identical external char surface reaction conditions, the apparent kinetics approach can lead to large errors when there are significant variations in the gas diffusivity. However, for moderate variations in gas diffusivity, as occur in oxy-fuel combustion compared to conventional combustion, the error in using an apparent char kinetic expression in the new environment should be minor. Assuming this effect scales linearly with the magnitude of the diffusivity, the 50% difference in absolute reaction rate observed here with a 3.5 times greater diffusivity will translate into a 3.4% difference in a CO_2 environment that has a 17% lower diffusivity. Given the uncertainty in determining char kinetic rates, this minor difference is unlikely to be experimentally distinguishable and can probably safely be ignored.

5. Conclusions

To investigate the influence of gas diffusivity on apparent char combustion kinetic rates, a comprehensive study was conducted involving char particle combustion temperature and burnout measurements, combined with detailed char particle combustion modeling, for char particles burning in an optical laminar entrained flow reactor with helium and nitrogen diluents. The combination of much higher thermal conductivity and mass diffusivity in the helium environments resulted in cooler char combustion temperatures than in equivalent N_2 environments. Measured char burnout was similar for a given bulk oxygen concentration but was approximately 60% higher in helium environments as a function of char combustion temperature. Detailed particle simulations with the SKIPPY code also showed a 60% higher burning rate in the helium environments for a given char particle combustion temperature. Additional SKIPPY simulations

were constructed that produced identical char combustion temperatures and particle surface concentrations of O_2 and steam reactants in He and N_2 bath gases, which necessitates identical apparent char burning rates. Under these conditions, despite similar oxygen penetration in the two diluents, the actual char burning rate was found to be 50% higher in He, demonstrating the limitations of apparent kinetics. However, when scaling these results to the case of oxy-fuel combustion, wherein the difference in diffusivities is much smaller, the apparent char oxidation rates will be lower, but probably by no more than a few percent.

Acknowledgments

Support for this research was provided by the U.S. Department of Energy through the National Energy Technology Laboratory's Cross-Cutting Research Program. The assistance of Dr. Jinhan Yun (KIMM, South Korea) in collecting char samples for this work is greatly appreciated. Sandia National Laboratories is a multimission laboratory managed and operated by National Technology and Engineering Solutions of Sandia, LLC., a wholly owned subsidiary of Honeywell International, Inc., for the U.S. Department of Energy's National Nuclear Security Administration under contract DE-NA-0003525. The views expressed in the article do not necessarily represent the views of the U.S. Department of Energy or the United States Government.

References

[1] M. A. Field, *Combust. Flame* 14 (1970) 237–248.

[2] I. W. Smith, *Proc. Combust. Inst.* 19 (1982) 1045–1065.

[3] L. D. Smoot, P. J. Smith, Coal Combustion and Gasification, Vol. 1, Springer US, 1985.

[4] E.W. Thiele, *Ind. Eng. Chem.* 31 (1939) 916–920.

[5] R. Hurt, J.K. Sun, M. Lunden, *Combust. Flame* 113 (1998) 181-197.

[6] J.J. Murphy, C.R. Shaddix, *Combust. Flame* 144 (2006) 710–729.

[7] M. Geier, C.R. Shaddix, K.A. Davis, H.-S. Shim, *Appl. Energy* 92 (2012) 675-679.

[8] X. Ge, J. Dong, H. Fan, Z. Zhang, X. Shang, Z. Hu, J. Zhang, *Fuel* 207 (2017) 602-614.

[9] K. Luo, Y. Bai, T. Jin, K. Qiu, J. Fan, *Energy Fuels* 31 (2017) 8742-8757.

[10] T.R. Marrero, E.A. Mason, *J. Phys. Chem. Ref. Data* 1 (1972) 3–118.

[11] J. Kestin, K. Knierim, E.A. Mason, B. Najafi, S.T. Ro, M. Waldman, *J. Phys. Chem. Ref Data* 13 (1984) 229–303.

[12] F.J. Uribe, E.A. Mason, J. Kestin, *J. Phys. Chem. Ref Data* 19 (1990) 1123–1136.

(1998) 1247-1251.

[13] L. Chen, S.Z. Yong, A.F. Ghoniem, *Prog. Energy Combust. Sci.* 38 (2012) 156-214.

[14] E. Hecht, C.R. Shaddix, A. Molina, B.S. Haynes, *Proc. Combust. Inst.* 33 (2011) 1699-1706.

[15] E. Hecht, C.R. Shaddix, M. Geier, A. Molina, B.S. Haynes, *Combust. Flame* 159 (2012) 3437–3447.

[16] C.R. Shaddix, Proceedings of the 33rd National Heat Transfer Conference, HTD99-282, ASME, New York, NY, 1999.

[17] P.J. Ashman, B.S. Haynes, Improved techniques for the prediction of NOx formation from char nitrogen, Project No. C4065; Australian Coal Association. CSIRO Energy Technology: North Ryde NSW, Australia, 1999.

[18] R.J. Kee, F.M. Rupley, J.A. Miller, CHEMKIN II: A Fortran Chemical Kinetics Package for the Analysis of Gas-Phase Chemical Kinetics. SAND 89-8009, Sandia National Laboratories, CA, 1989.

[19] M.E. Coltrin, R.J. Kee, F.M. Rupley, Surface Chemkin (Version 3.7): A Fortran Package for Analyzing Heterogeneous Chemical Kinetics at a Solid-Surface-Gas-Phase Interface. SAND90-8003, Sandia National Laboratories, CA, 1990.

[20] R.J. Kee, G. Dixon-Lewis, J. Warnatz, M.E. Coltrim, J.A. Miller, A Fortran Computer Code Package for the Evaluation of Gas-Phase, Multicomponent Transport Properties. SAND 86-8246, Sandia National Laboratories, CA, 1986.

[21] J.F. Grcar, *The twopnt program for boundary value problems*, SAND-91-8230; Sandia National Labs: Livermore, CA, (USA), 1992.

[22] G.P. Smith, S.D. Golden, M. Frenklach, N.W. Moriarty, B. Eitener, M. Goldenberg, C.T. Bowman, R.K. Hanson, S. Song, W.C. Gardiner, V.V. Lissianski, Z. Qin, GRI-MECH 3.0, 2001. <http://www.me.berkeley.edu/gri_mech> (accessed 12.10).

[23] C.R. Shaddix, A. Molina, *Proc. Combust. Inst.* 32:2091-2098 (2009).